Journal of Membrane Science & Research

Research Paper

Fouling Mechanism Study of Nanoporous Membrane by Ultrafitration of Whey Proteins

Fatemeh Esfandian, Majid Peyravi*, Ali Asqar Qoreyshi, Mohsen Jahanshahi

Membrane Research Group, Nanobiotechnology Institute, Babol University of Technology, Babol, Iran

ARTICLE INFO

KEYWORDS

GRAPHICAL ABSTRACT

HIGHLIGHTS

• Developing structural characteristics of PSf membrane
• Assessment of fouling behavior during whey ultrafiltration
• Presenting chemistry based concept for the membrane fouling mechanism

ABSTRACT

One of the barriers during whey filtration using UF membrane is the fouling phenomenon of the membrane, which is caused by whey proteins. In this work, the UF membranes were prepared using polysufone (PSf), dimethyl formamide (DMF), 1 wt.% poly vinyl pyrrolidone (PVP) and different concentrations of LiCl via phase inversion induced by immersion precipitation. The prepared membranes were characterized using SEM, AFM, porosity and mean pore size measurements, ultrafiltration performance and fouling analysis. The roughness of the membrane surface increased after the addition of LiCl in the casting solution. The SEM images and the measured data of porosity and pore size showed that the porosity was significantly enhanced after modification with LiCl but the pore sizes of the membrane were reduced. The performance analysis of these membranes demonstrated that the modified membranes had higher pure water and whey flux in comparison to the neat membrane and all of the prepared membranes exhibited protein rejection higher than 90%. In order to evaluate the membrane fouling, the experimental fouling analyses were carried out and the Zedney's pore blockage and cake filtration model was employed. The membranes fouling in terms of pore-blocking slightly decreased after the addition of LiCl.

1. Introduction

Whey is the main by-product of the dairy industry obtained from cheese production. Considering the high organic contents of cheese whey, it is known as a wastewater with high pollution which must be treated before discharge to the environment. Otherwise, it can be used as animal food to avoid the waste treatment costs [1]. Cheese whey contains a high concentration of valuable components, such as protein and lactose that can be recovered using an appropriate technique. Depending on the milk properties and the technology used for cheese production, whey composition can be varied. Generally, it contains 5–6% lactose, 0.8–1% protein and 0.06% fat. It is considered as one of the most important biological sources of proteins (contains about 20% of the total proteins in milk) [2-5]. Due to the presence

* Corresponding author at: Phone: +98 1132 320342, Fax: +98 1132 320342
E-mail address: majid.peyravi@nit.ac.ir (M. Peyravi)

of valuable components in whey, recovery of these components from whey not only improves the overall efficiency of cheese production in the dairy industry, but also may be regarded as a solution for the wastewater treatment problem and reduction of water contamination. Whey proteins are typically a mixture of beta-lactoglobulin (~65%), alpha-lactalbumin (~25%), bovine serum albumin (~8%) and immunoglobulins. Whey proteins have a high nutritional value. They have excellent functional properties when they are used as components in food, mainly due to their high solubility, water absorption, and gelatinization and emulsifying volumes [6, 7].

Membrane processes, especially ultrafiltration, are known as an important and efficient method for recovery of whey proteins [8]. Ultrafiltration is a pressure-driven process that separates particles of one size from particles of another size in a suspending solution using a filter. It is especially used in industry and scientific research for purifying and concentrating macromolecules [9, 10]. In the dairy industry, ultrafiltration is used for a wide range of applications such as fractionating the proteins from whey and fresh cheese production from ultrafiltered milk. Application of ultrafiltration in the dairy industry dates back to the separation and concentration of whey proteins from whey in 1972 [11, 12]. Most ultrafiltration membranes retain the majority of proteins in milk or whey, but permit smaller sized components such as lactose, soluble salts and non-protein nitrogen fractions to pass through the membranes along with the permeate.

Generally, fouling is caused by deposition and adsorption of particles and compounds on the surface of the membranes and membrane pores during filtration. It depends on the nature of the interaction between the feed components and the membrane. UF fouling generally happens through several mechanisms including adsorption, pore blocking and cake or gel formation [13-16]. Fouling is a major factor that can limit the membrane flux and increase operation costs. Recent development in understanding membrane fouling can be summarized in four basic aspects: 1) recognition of major components (e.g., protein) that are mainly responsible for the fouling of UF membranes, 2) development of phenomenological models for membrane fouling, 3) establishment of mathematical models to describe or predict fouling, and 4) development of fouling control strategies.

Whey is a severe foulant in the membrane ultrafiltration process that has been employed in our work as a model feed for investigating the fouling mechanism of the membrane. The fouling mechanism related to the proteins of whey is attributed to the adsorption and deposition of these proteins onto the membrane surface, which act as a flux resistance [17].

Table 1. The whey characteristic of kalleh factory

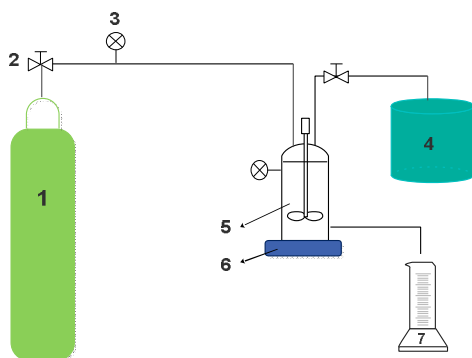| Parameters	Value
PH	5-6
Proteins (g/l)	4-6
Lactose (g/l)	60
Conductivity (mS/cm)	6.05
Total dissolved solids (mg/l)	2940

Fig .1. Scheme of the dead-end filtration system: (1) cylinder with compressed nitrogen, (2) pressure safety valve, (3) pressure gauge, (4) feed tank, (5) membrane cell, (6) magnetic stirrer, (70) permeate collector.

Low molecular weight inorganic salts (such as LiCl) are particularly interesting additives for membrane preparation to improve the membrane morphology and properties since the inorganic salts strongly interact with carbonyl groups in polar solvents such as dimethylformamide and the formed

complexes would increase the viscosity of casting solution and affect the membrane's structure [18]. Fontananova et al. [19] found that the addition of LiCl in the PVDF/dimethylacetamide dope increases flux of the casted membranes at a low LiCl concentration of 2.5 wt.%, but it suppressed macrovoid formation at a high concentration of 7.5% LiCl and resulted in a decrease of the membrane permeation flux. Similar results were obtained by Lee et al. [20]. They found that by increasing LiCl concentration in the PAA/N-methyl-2-pyrrolidone system, the solution viscosity could be raised to the point where macro-void formation is hindered and formed a membrane with a porous structure.

Here, we focused on the estimation of fouling phenomena via changing structural properties of the membrane for whey ultrafiltration. In this regard, inorganic salt (LiCl) was used as pore forming additives to improve the structural properties of the membrane. To the best of our knowledge, a theoretical predictive model was utilized for determination of the role of pore blockage and cake layer formation as a dominant resistant during whey filtration.

2. Experimental

2.1. Material

Polysulfone (PSF, Mw=35,000 g/mol, Density=1.24 g/mL at 25 °C) was used as the basic polymer for the preparation of the ultrafiltration membrane. Polyvinylpyrrolidone (PVP, with Mw=25,000 g/mol, Density=1.2 g/mL at 20 °C), LiCl and N, N dimethylformamide (DMF) as solvent was supplied from Merck. Whey was supplied from Kalleh factory dairy products (Amol-Iran) and the characteristics of fresh cheese whey were presented in Table 1.

2.2. Preparation of ultrafiltration membranes

The flat sheet membranes were prepared by phase inversion via the immersion precipitation technique. The blend homogenous solutions were prepared by dissolving 16wt. % of PSf and 1 wt.% of PVP in DMF at a temperature of 60 °C for 12 h with magnetic stirring. Separately, different concentrations of LiCl (0, 0.1, 0.5, 1 wt.%) were dissolved at certain amounts of DMF with a magnetic stirrer for 1 h. PSF solution was then dissolved in a mixture of LiCl and DMF. The solution was sprinkled and casted on the polyester non-woven fabric using a homemade casting knife with 70 μm thickness. This solution was immediately moved to the non-solvent bath containing only water at room temperature without any evaporation. The non-solvent was only water. The prepared membranes were washed and stored at 25 °C distilled water for 1 day to completely leach out the residual solvents and additives. At the final stage, the membranes were dried by placing them between two sheets of filter paper for 24 h at room temperature. The compositions of the casting solution are given in Table 2.

2.3. Characterization of membranes

The morphological studies were accomplished by scanning electron microscopes (SEM) and atomic force microscopy (AFM). SEM was used to inspect the cross-section and surface of the membranes. The membranes were cut into pieces of small sizes and cleaned with filter paper. These pieces were immersed in liquid nitrogen for 10–15 s and were frozen. Frozen bits of the membranes were broken and kept in air for drying. AFM was used to analyze the surface morphology and roughness of the prepared membranes. This device was a Nanosurf scanning probe optical microscope (EasyScan II, Swiss). The surface roughness parameters of the composite membranes which are expressed in terms of the mean roughness (Sa), the root mean square of the Z data (Sq) and the mean difference between the five highest peaks and lowest valleys (Sz) were calculated from AFM images using the tapping mode method via Nanosurf Easy Scan software at a scan area of 10 μm × 10 μm.

Table 2. Composition of casting solution.

Membrane	PSf (wt.%)	PVP (wt.%)	LiCl (wt.%)	DMF (wt.%)
M_0	16	1	0	83
$M_{0.1}$	16	1	0.1	82.9
$M_{0.5}$	16	1	0.5	82.5
M_1	16	1	1	82

Equilibrium water content (EWC) is considered to be a main characterization parameter that indicates the degree of hydrophilicity and hydrophobicity of a membrane [21]. Moreover, it is related to the porosity of

a membrane. To determine EWC, first a piece of dry membrane was weighed by an electronic balance. Then, it was soaked in water for 24 h. The weight of the wet membrane after mopping the surface water with blotting paper was obtained once more by the same electronic balance. Then EWC is calculated as follows:

$$EWC(\%) = \frac{W_w - W_d}{W_w} \times 100 \tag{1}$$

where W_w is the wet membranes weight (g) and W_d is the dry membranes weight (g). The membrane porosity ε is the ratio of the volume of pores to total volume of the porous membrane and is obtained by Equation (2) [22]:

$$\varepsilon = \frac{W_w - W_d}{\rho_w \times AL} \tag{2}$$

where, ρ_w is pure water density (kg/m³) at room temperature. A and L are membrane area and membrane thickness, respectively.

The membrane mean pore radius (r_m) was measured by the pure water flux and porosity data. r_m was calculated by the following formula [23].

$$r_m = \sqrt{\frac{(2.9 - 1.75\varepsilon) \times (8\eta l Q)}{\varepsilon \times A \times \Delta P}} \tag{3}$$

where η is the water viscosity (8.9×10^{-4} Pa·s), Q is water flux (m³/s) and ΔP is the operation pressure (3×10^5 Pa).

2.4. Filtration performance and fouling analysis

The filtration experiments were carried out using a laboratory-scale dead-end system as shown in Figure 1. The feed flow was passed through the membrane by a pressure driving force, which was provided by a compressed nitrogen gas cylinder. A membrane with radius of 5 cm was fixed between two steel parts and was also sealed with an O-ring. A magnetic stirrer was also located under the membrane cell to stir feed in order to reduce the concentration polarization effect. After the membrane was fixed, the stirred cell and the solution reservoir were filled with deionized water to measure the pure water flux (J_{w0}). After 15 min of filtration, the feed solution was switched from water to the whey, and the flux (J_p) was measured periodically. Finally, the cell and the solution reservoir were fully emptied and refilled with deionized water. The membrane was washed with deionized water for 10 min and the water flux (J_{w1}) was measured again. Flux and rejection of all membranes were determined under 3 bar trans-membrane pressure (TMP) at a temperature of 25 °C. Fluxes of different membranes were calculated as follows:

$$J = \frac{m}{A.\Delta t} \tag{4}$$

where, m (kg) is the mass of permeate, A (m²) the membrane area and Δt (h) the permeation time. The protein rejection ratio was calculated by the following equation:

$$R(\%) = \left(1 - \frac{C_p}{C_f}\right) \times 100 \tag{5}$$

where C_p and C_f represented proteins concentrations in permeate and feed solutions, respectively measured by the UV–vis spectrometer at a wavelength of 287 nm.

Fouling can be quantified by the resistance which appears during the filtration process. The reversible fouling (R_r) relies on the concentration polarization and formation of cake while the irreversible fouling (R_{ir}) is attributed to the pore-blocking effect. These two types of fouling are exhibited in Figure 2. In order to evaluate the fouling-resistant property of the membrane, the flux recovery ratio (FRR) was calculated using the following expression:

$$FRR(\%) = \frac{J_{w1}}{J_{w0}} \times 100 \tag{6}$$

The fouling-resistant capability of the membrane was described by:

$$R_t = \frac{J_{w0} - J_p}{J_{w0}} \tag{7}$$

R_t is the degree of total flux loss caused by total fouling. Reversible fouling ratio (R_r) and irreversible fouling ratio (R_{ir}) were also defined and calculated by the following equations, respectively.

$$R_r = \frac{J_{w1} - J_p}{J_{w0}} \tag{8}$$

$$R_{ir} = \frac{J_{w0} - J_{w1}}{J_{w0}} \tag{9}$$

Obviously, R_t was the sum of R_r and R_{ir}.

2.5. Combined pore-blockage and cake-filtration model

A variety of models are commonly used to predict the flux rate through ultrafiltration membranes. In this paper, flux decay curves were analyzed using the model presented by Ho and Zydney for protein microfiltration [24]. This model accounts for both pore blockage and cake formation at the same time. In this model, the initial flux decline is considered to be due to the blockage of membrane pores by physical deposition of large aggregates on the pore mouths and membrane surface. α is the pore blockage parameter that is equal to the membrane pore area blocked per unit mass of protein convected to the membrane surface. In this method, the normalized flux can be explained as a function of filtration time with a constant coefficient as follows:

$$\frac{J}{J_0} = \exp\left(-\frac{\alpha \Delta P C_b}{\mu R_m} t\right) + \frac{R_m}{R_m + R_p}\left[1 - \exp\left(-\frac{\alpha \Delta P C_b}{\mu R_m} t\right)\right] \tag{10}$$

where J_0 and J (m³/s) are volumetric filtrate flow rates at the initial and end of filtration time, respectively. α (m²/kg) is considered as a pore blockage parameter and shows the blocked membrane area per unit mass of aggregates connected to the membrane. C_b (kg/m³) is the bulk concentration of proteins; ΔP is the transmembrane pressure (Pa). R_p is the resistance of protein layer on the membrane surface that can be assumed constant over the period of filtration time. Also, Ho and Zedney assumed a uniform maximum resistance of protein layer through the fouled surface of the membrane. R_m is the resistance of the clean membrane that was calculated using the following expression [25]:

$$R_m = \frac{\Delta P}{\mu J_{w0}} \tag{11}$$

where μ is the viscosity of the permeate. The flow rate can be controlled by three parameters: a pore blockage parameter, α, the resistance of the protein deposit, Rp, and the resistance of clean membrane parameter, R_m.

The right hand side of Equation (10) includes two terms that show the effect of pore blockage and cake formation, respectively. The first term (pore blocking) dominates at the early stage of fouling, and the second term (cake filtration) will be the controlling parameter at longer times [26]. To realize the difference in fouling behavior, the normalized flow rate data, which were obtained experimentally were fitted to the exponential form of Equation (10) using Sigma Plot software version 12 (Systat Software, Inc., Canada). The theoretical curves were generated by Sigma Plot software via fitting the exponential decay (3 parameters) equation (Equation (12)) with R^2 of 0.90–0.99.

$$y = y_0 + ae^{-bt} \tag{12}$$

3. Results and discussion

3.1. Effect of LiCl on membrane morphology

For the morphological study of membranes, the surfaces of PSf ultrafiltration membranes prepared with different concentrations of LiCl were evaluated by AFM. Figure 3 shows the two and three-dimensional surface AFM images, which cover an area of 5 μm × 5 μm. Surface roughness of the LiCl-modified membranes was higher in comparison to the unmodified membrane which could be as a consequence of LiCl aggregation onto the membrane surface during the phase inversion process [27]. In other words, the phase inversion process diffuses out the solvent from the casted film and carries the LiCl salts to the surface of the membrane. As a result of this process, the LiCl salts aggregate onto the surface and increase the surface roughness of the membrane. The Gaussian curve was fitted to the pore size distribution diagrams and the curves were shown in Figure 3. The narrow

pore size distribution was observed for M_0 and the pore size of M_0 was higher than $M_{0.5}$.
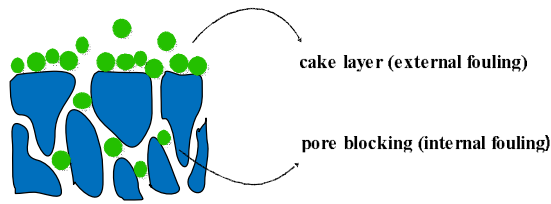

Fig .2. Exhibition the membrane fouling, cake layer formation and pore blocking.

The surface roughness parameters of the membrane which are considered as the mean roughness (S_a), the root mean square of z data (S_q) and the mean difference between the highest peaks and lowest valleys (S_z) were calculated in 5 µm ×5 µm scan size and are listed in Table 3. The tabulated values of roughness parameters confirm that the roughness of the membrane surface increased with the addition of 0.5 wt. % LiCl in the casting solution. The roughness parameters depend on the Z-value (the vertical distance which the piezoelectric scanner moves). When the surface contains deep valleys and high peaks, the tip moves up and down over a wide range which increases the

roughness parameter of the membrane surface.

Figure 4 presents the cross-section SEM images of prepared membranes with 0 and 0.5 wt. % LiCl (M_0 and $M_{0.5}$). These membranes exhibited an asymmetric structure consisting of the dense sub-layer and fully developed finger-like pores at the bottom. The macro-voids with finger-like structure were observed in the cross-section SEM image of M_0 whereas macro-voids became larger and extended over the whole cross-section when 0.5 wt. % LiCl was added to the casting solution. Comparing the M_0 and $M_{0.5}$ cross-section SEM images, it can be seen that $M_{0.5}$ almost showed a sponge-like structure with more porosity. LiCl possesses strong interactions with the components of the casting solution. These interactions tend to delay the dope precipitation, which causes the formation of a membrane with a sponge-like structure [19]. The surface SEM images of $M_{0.5}$ are presented in Figure 5. The porous structure was observed at the top surface of $M_{0.5}$. This surface image of $M_{0.5}$ showed the porous structure of the top surface. In addition, the surface of this membrane also showed some defects at higher magnification.

The porosity and mean pore size of the membranes are tabulated in Table 4. According to the listed value, the porosity of LiCl-modified membranes was improved after modification with LiCl. However, a decrease in the mean pore size of the membranes was observed by increasing the LiCl content to 1 wt.%. This can be attributed to the affinity between non-solvent and LiCl that alters the exchange rate between solvent and non-solvent during the phase separation process which formed a membrane with smaller pore size [28].
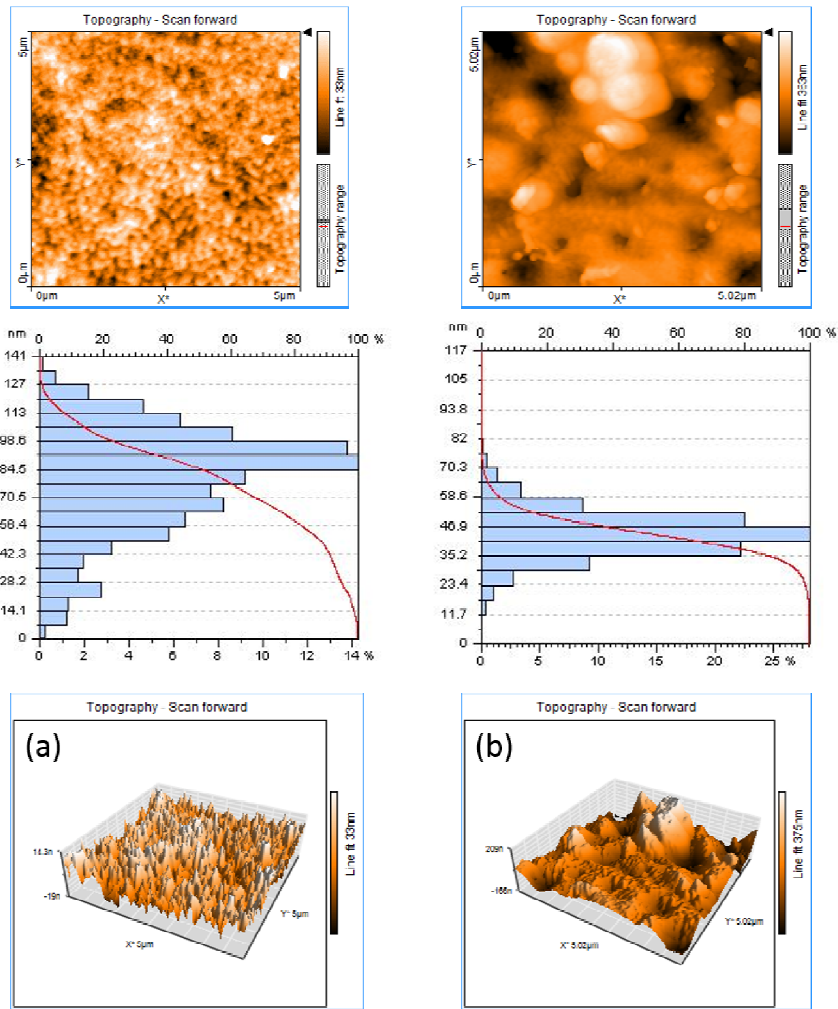

Fig. 3. 2 and 3-dimensional surface AFM images of membranes prepared with (a) 0 wt. % (b) 0.5 wt. % LiCl.

3.2. Membrane performance

Pure water flux of the membranes prepared with different concentrations of LiCl was measured using clean and fouled membranes after whey filtration. The obtained results of these experiments are shown in Figure 6. Before filtration of the whey (for the clean membrane), the pure water flux of modified membranes with LiCl were increased by increasing the LiCl

content. Among the fabricated membranes with different contents of LiCl, a maximum value of pure water flux was observed for the membrane with 0.5 wt.% LiCl. Increasing the concentration of LiCl beyond 1 wt.% in the casting solution strongly reduced the pure water flux to 23.823 kg/m^2.h. The authors believe that the flux decline for M_1 is due to the reduction of pore size. Indeed, the addition of LiCl to the membrane structure, increased porosity and decreased membrane pore size. It seems that the effect of membrane pore size

dominates the porosity effect for the case of the M_1 membrane.

The flux of whey through modified membranes was higher than the neat membrane except for M_1. This may be attributed to the higher porosity after modification. However, increasing the LiCl contents decreased the whey flux for the modified membrane. This indicates that reduction of the membrane pore size is more effective than the porosity enhancement.

Table 3. Surface roughness parameters of membranes.

Membrane	Roughness		
	S_a (nm)	S_q (nm)	S_z (nm)
M_0	4.2994	5.4226	50.533
$M_{0.5}$	48.334	65.569	455.63

Table 4. Porosity and mean pore radius of membranes.

Membrane	Porosity	Mean pore size (nm)
M_0	0.57857	10.1014
$M_{0.1}$	0.696	11.0799
$M_{0.5}$	1.096	7.1835
M_1	1.27857	2.387

Table 5. Flux recovery ratio and resistances of membranes.

Membrane	J_p(kg/m^2.h)	FRR (%)	R_r	R_{ir}
M_0	13.248	42.70	0.23167	0.5728
$M_{0.1}$	21.94	48.64	0.293	0.5136
$M_{0.5}$	18.2144	34.65	0.2005	0.6535
M_1	3.728	19.19	0.354	0.8081

Table 6. R^2 value, pore blockage parameter and resistance of clean membrane.

Membrane	R^2	α (m^2/kg)	R_m(×10^{13} m^{-1})
M_0	0.89	1.7705	1.7824
$M_{0.1}$	0.92	0.946	1.097
$M_{0.5}$	0.987	1.295	0.968
M_1	0.96	13.279	5.071

The effects of LiCl in the casting solution on a long term whey flux and rejection were represented in Figures 7 and 8, respectively. As shown in Figure 7, the flux decline at the initial period of whey filtration can be attributed to the pore plugging of the membrane as a consequence of the partial obstruction of the pore entrance or pore bridging [29, 30]. For $M_{0.5}$ and M_1 a slight flux decline was observed which was due to the smaller pore size distribution. In fact, the solutes with sizes of more than the pore diameter cannot enter and pass through the pore. Therefore, pore blocking did not occur at the initial period of filtration and the fouling may be controlled by other mechanisms. Figure 7 illustrates that the flux decline of the neat membrane is very high in comparison to the modified membranes. This may be due to the fact that the formation of a cake layer on the surface of the modified membranes was low during the long-term filtration since these membranes had more porosity and therefore more particles can pass through the membrane.

Figure 8 shows that in spite of the higher flux observed for the modified membrane compared to the neat membrane, the protein rejection is not decreased and almost remains unchanged. Moreover, protein rejection for M_1 was increased to 99.16% because of the smaller pore size.

3.3. Fouling behavior

To investigate the fouling behavior of the synthesized membranes, the flux recovery ratio, reversible and irreversible resistance of neat and modified membranes were calculated and listed in Table 5. The higher flux recovery ratio (FRR) indicates the superior property for the membrane [31]. Among the modified membranes, a membrane with 0.1 wt.% LiCl had the maximum value of FRR. This can be attributed to its highest mean pore size among the membranes modified with different contents of LiCl. For this reason, the pore blockage of this membrane was less than other membranes. It should also be noted that FRR declined at the high concentrations of additives, which might also be as a result of pore blockage [30]. It can be seen that the irreversible resistance (R_{ir}) of the membrane with 0.1 wt.% LiCl is low compared to other

membranes. This may be due to the fact that the membranes with larger mean pore size have lower tendency to adsorb protein, resulting in a lower pore blockage for the membrane. R_r relies on the concentration polarization and formation of cake on the membrane surface. Since R_r increases and R_{ir} decreases, the membrane shows a better performance in terms of fouling because the reversible fouling can be reduced by simple methods including backwashing with de-ionized (DI) water, chemical cleaning, and sonication [32].
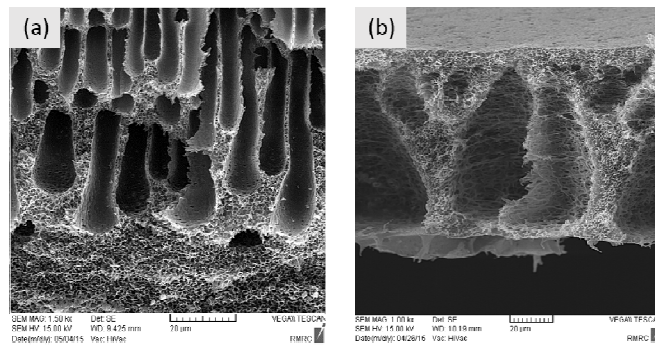

Fig. 4. Cross section SEM image of membrane with (a) 0 wt. % LiCl (b) 0.5 wt. % LiCl.

3.4. Model calculations

In the present study, Zedney's model [24] was employed to analyze the fouling mechanism in the membranes that occurred during the ultrafiltration test with whey solution. Figure 9 shows the fitting of the combined pore blockage and cake filtration model with experimental results (normalized flux) during ultrafiltration of the cheese whey solution. As shown in Figure 9, the flux decline was observed during long time filtration. The normalized flux curve at Zedney's work [24] declined with a steep slope in comparison to our work and a severe flux reduction was observed during 20 min of protein filtration at Zedney's work. In addition, the range of normalized flux at Zedney's work was more than our work during the 60 min filtration. This lower flux reduction was probably due to the fact that the aggregation and adsorption of molecules in the interior of our membrane was lower than Zedney's work.
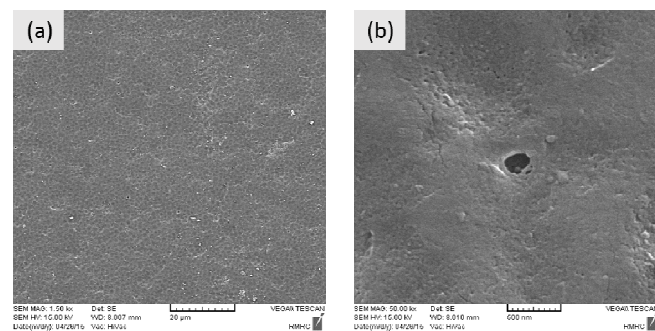

Fig. 5. Surface SEM image of membrane with 0.5 wt.% LiCl; Scale bar for images (a) is 20 µm and (b) is 500 nm.
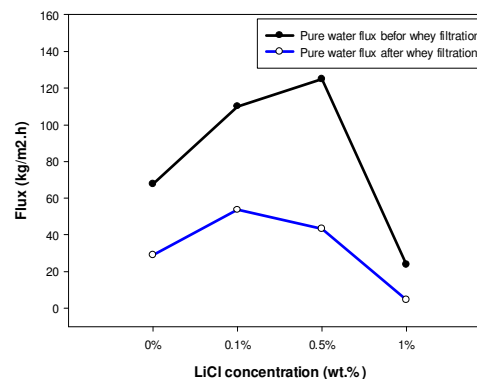

Fig. 6. Pure water flux of membranes before and after whey filtration.

The parameters of this model were obtained using Sigma Plot software via Equation 12. Table 6 tabulated the values of R^2, calculated pore blockage parameter (α) and R_m. In Table 6, the highest R^2 was observed for $M_{0.5}$. As a matter of fact, Figure 9 clearly showed that the best prediction was obtained for $M_{0.5}$. A maximum value of pore blockage parameter was obtained for the membrane prepared with 1% LiCl because of the smaller mean pore size and denser structure than others. A comparison of the modified and neat membrane indicated that the pore blockage parameter (α) of the membrane was decreased after modification with LiCl. However, for the unmodified membrane, hydrophobic interaction between the protein and membrane might be a reason for the high value of pore blockage parameter. It seems that the effect of hydrophobic interaction was decreased after modification due to the ionic composition of LiCl. Among modified membranes, the pore blockage parameter increased with increasing the LiCl content as a consequence of the mean pore size decline.
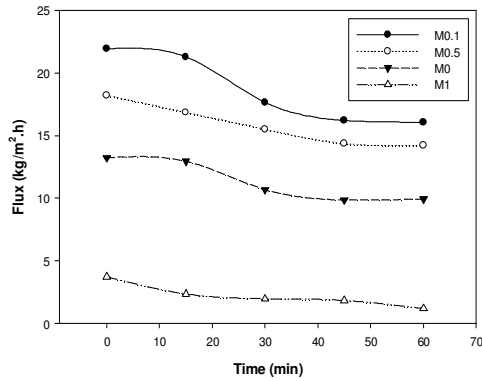
over the long-term operation of whey UF processes. The model fit well to experimental data. According to the obtained results from the fouling study, the pore blocking of the membrane with 0.1 wt.% LiCl is lower than other membranes.
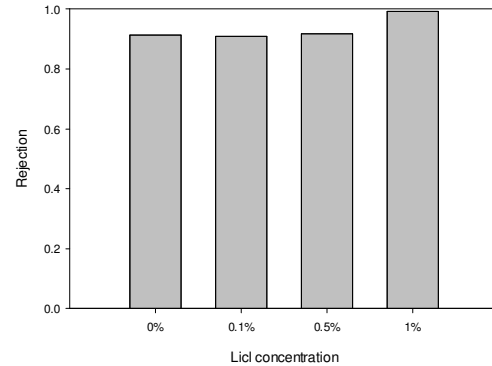

Fig. 8. Protein rejection of different membranes.

Fig. 7. Flux of different membranes during filtration of whey.

4. Conclusion

In this work ultrafiltration membranes were prepared using the phase inversion precipitation technique by the addition of different components such as PVP, LiCl and DMF in the casting solution. Membranes characterization demonstrated that the presence of LiCl at different concentrations had important effects on the membranes structure such as mean pore size and porosity and surface roughness. The results demonstrated that membrane porosity was increased by increasing LiCl content. Morphological analysis demonstrated that a rougher surface appeared for $M_{0.5}$ than M_0. Moreover, these membranes were used for whey proteins separation and the membrane performance was investigated in terms of flux, rejection and fouling during whey filtration. The flux of whey and pure water for the modified membranes was higher than the neat membrane except for M_1. In addition to experimental data, Zedney's model was applied to describe the fouling and flux decline

Nomenclature

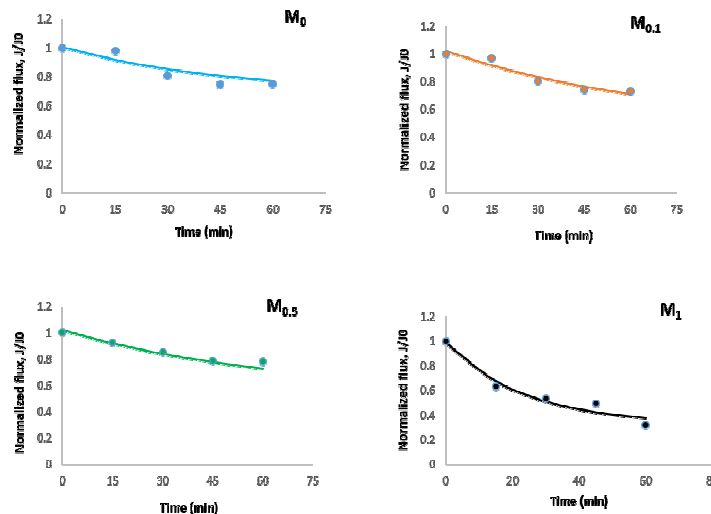|	
E	Membrane porosity
r_m	Membrane mean pore radius (nm)
C_p	Proteins concentration of feed (mg/ml)
C_f	Proteins concentration of permeate (mg/ml)
R	Proteins rejection ratio
J	Permeate flux (l/m².h)
H	Water viscosity (Pa.s)
R_{ir}	Irreversible fouling ratio
R_r	Reversible fouling ratio
R_t	Total fouling ratio
FRR	Flux recovery ratio
A	Membrane area (cm²)
L	Membrane thickness (cm)
ΔP	Operation pressure (Pa)
Sa	Mean roughness (nm)
S_q	Root mean square of the Z data (nm)
S_z	Mean difference between the highest peaks and lowest valleys (nm)
A	Pore blockage parameter (m²/kg)
C_b	Bulk concentration of proteins (kg/m³)
R_m	Resistance of clean membrane (m⁻¹)
J_0	Volumetric filtrate flow rates at the initial time of filtration (m³/s)

Fig. 9. Normalized flux of different membranes; Colored curves are model calculation using equation (10).

References

[1] K. Pan, Q. Song, L. Wang, B. Cao, A study of demineralization of whey by nanofiltration membrane, Desalination 267 (2011) 217–221.

[2] M.S. Yorgun, I. Akmehmet Balcioglu, O. Saygin, Performance comparison of Ultrafiltration, nanofiltration and reverse osmosis on whey treatment, Desalination 229 (2008) 204–216.

[3] E. Suárez, A. Loboa, S. Álvarez, F.A. Riera, R. Álvarez, Partial demineralization of whey and milk ultrafiltration Permeate by nanofiltration at pilot-plant scale, Desalination 198 (2006) 274–281.

[4] A. Hinkova, P. Zidova, V. Pour, Z. Bubnik, S. Henke, A. Salova, P. Kadlec, Potential of membrane separation processes in cheese whey fractionation and separation, Procedia Eng. 42 (2012) 1425–1436.

[5] R. Rosa de Souza, R. Bergamasco, S. Claudio da Costa, X. Feng, S. Henrique Bernardo Faria. M.L. Gimenes, Recovery and purification of lactose from whey, Chem. Eng. Process. 49 (2010) 1137–1143.

[6] C. Baldasso, T.C. Barros, I.C. Tessaro, Concentration and purification of whey proteins by ultrafiltration, Desalination 278 (2011) 381–386.

[7] I. Barukcic, R. Bozanic, U. Kulozik, Effect of pore size and process temperature on flux, microbial reduction and fouling mechanisms during sweet whey cross-flow microfiltration by ceramic membranes, Int. Dairy J. 39 (2014) 8-15.

[8] A. Rahimpour, M. Jahanshahi, A. Mollahosseini, B. Rajaeian, Structural and performance properties of UV-assisted TiO_2 deposited nano-composite PVDF/SPES membranes, Desalination 285 (2012) 31–38.

[9] L. Ding, O. Al-Akoum, A. Abraham, M.Y. Jaffrin, Milk protein concentration by ultrafiltration with rotating disk modules, Desalination 144 (2002) 307-311.

[10] W.J. Koros, Y.H. Ma, T. Shimidzu, Terminology for membranes and membrane processes, J. Membr. Sci. 120 (1996) 149-302.

[11] B. Cuartas-Uribe, M.I. Alcaina-Miranda, E. Soriano-Costa, J.A. Mendoza-Roca, M.I. Iborra-Clar, J. Lora-García, A study of the separation of lactose from whey ultrafiltration permeate using nanofiltration, Desalination 241 (2009) 244-255.

[12] R. Atra, G. Vatai, E. Bekassy-Molnar, A. Balint, Investigation of ultra- and nanofiltration for utilization of whey protein and lactose, J. Food Eng. 67 (2005) 325–332.

[13] H.P. Hsieh, Inorganic membranes for separation and reaction, Elsevier B.V., Amsterdam, The Netherlands, 1996, pp.186- 187.

[14] N. Norazman, W. Wu, H. Li, V. Wasinger, H. Zhang, V. Chen, Evaluation of chemical cleaning of UF membranes fouled with whey protein isolates via analysis of residual protein components on membranes surface, Sep. Purif. Technol. 103 (2013) 241–250.

[15] A. Makardij, X.D. Chen, M.M. Farid, Microfiltration and ultrafiltration of milk: some aspects of fouling and cleaning, J. Food Eng. 77 (1999) 107-113.

[16] B.J. James, Y. Jing, X.D. Chen, Membrane fouling during filtration of milk-a microstructural study, J. Food Eng. 60 (2003) 431–437.

[17] S.S. Madaeni, Y. Mansourpanah, Chemical cleaning of reverse osmosis membranes fouled by whey, Desalination 161 (2004) 13-24.

[18] A. Bottino, G. Capannelli, S. Munari, A. Turturro, High performance ultrafiltration membranes cast from LiCl-doped solutions, Desalination 68 (1988) 167-177.

[19] E. Fontananova, J.C. Jansen, A. Cristiano, E. Curcio, E. Drioli, Effect of additives in the casting solution on the formation of PVDF membranes, Desalination 192 (2006) 190–197.

[20] H.J. Lee, J. Won, H. Lee, Y.S. Kang, Solution properties of poly(amic acid)-NMP containing LiCl and their effects on membrane morphologies, J. Membr. Sci. 196 (2002) 267–277.

[21] G. Arthanareeswaran, C.S. Latha, D. Mohan, M. Raajenthiren, K. Srinivasan, Studies on cellulose acetate/low cyclic dimmer polysulfone blend ultrafiltration membranes and their application, Sep. Sci. Technol. 41 (2006) 2895–2912.

[22] B. Chakrabarty, A.K. Ghoshal , M.K. Purkait, Effect of molecular weight of PEG on membrane morphology and transport properties, J. Membr. Sci. 309 (2008) 209–221.

[23] G. Wu, Sh. Gan, L. Cui, Y. Xu, Preparation and characterization of PES/TiO_2 composite membranes, J. Appl. Surf. Sci. 254 (2008) 7080–7086.

[24] C.C. Ho, A.L. Zydney, A combined pore blockage and cake filtration model for protein fouling during microfiltration, J. Colloid. Interface Sci. 232 (2000) 389–399.

[25] A. Rahimpour, S.S. Madaeni, M. Jahanshahi, Y. Mansourpanah, N. Mortazavian, Development of high performance nano-porous polyethersulfone ultrafiltration membranes with hydrophilic surface and superior antifouling properties, J. Appl. Surf. Sci. 255 (2009) 9166–9173.

[26] C.-C. Ho, A.L. Zydney, Transmembrane pressure profiles during constant flux microfiltration of bovine serum albumin, J. membr. Sci. 209 (2002) 363-377.

[27] N. Niksefat, M. Jahanshahi, A. Rahimpour, The effect of SiO_2 nanoparticles on morphology and performance of thin film composite membranes for forward osmosis application, Desalination 343 (2014) 140–146.

[28] H. Yu, X. Zhang, Y. Zhang , J. Liu, H. Zhang, Development of a hydrophilic PES ultrafiltration membrane containing SiO2@N-Halamine nanoparticles with both organic antifouling and antibacterial properties, Desalination 326 (2013) 69–76.

[29] A. Rahimpour, M. Jahanshahi, S. Khalili, A. Mollahosseini, A. Zirepour, B. Rajaeian, Novel functionalized carbon nanotubes for improving the surface properties and performance of polyethersulfone (PES) membrane, Desalination 286 (2012) 99–107.

[30] A. Mehrparvar, A. Rahimpour, M. Jahanshahi, Modified ultrafiltration membranes for humic acid removal, J. Taiwan Inst. Chem. Eng. 45 (2013) 275–282.

[31] M. Peyravi, A. Rahimpour, M. Jahanshahi, A. Javadi, A. Shockravi, Tailoring the surface properties of PES ultrafiltration membranes to reduce the fouling resistance using synthesized hydrophilic copolymer, Microporous Mesoporous Mater. 160 (2012) 114–125.

[32] M. Peyravi, A. Rahimpour, M. Jahanshahi, Developing nanocomposite PI membranes: Morphology and performance to glycerol removal at the downstream processing of biodiesel production, J. Membr. Sci. 473 (2015) 72-84.